Optical Activity in Twisted Solid-Core Photonic Crystal Fibers

X. M. Xi,[1] T. Weiss,[1] G. K. L. Wong,[1] F. Biancalana,[1,5] S. M. Barnett,[3] M. J. Padgett,[4] and P. St. J. Russell[1,2]

[1]*Max Planck Institute for the Science of Light, Guenther-Scharowsky Strasse 1, 91058 Erlangen, Germany*
[2]*Department of Physics, University of Erlangen-Nuremberg, Staudtstrasse 7, 91058 Erlangen, Germany*
[3]*Department of Physics, University of Strathclyde, Glasgow G4 0NG, United Kingdom*
[4]*Department of Physics, University of Glasgow, Glasgow G12 8QQ, United Kingdom*
[5]*School of Engineering and Physical Sciences, Heriot-Watt University, Edinburgh EH14 4AS, United Kingdom*

(Received 21 December 2012; published 4 April 2013)

In this Letter we show that, in spectral regions where there are no orbital cladding resonances to cause transmission loss, the core mode of a continuously twisted photonic crystal fiber (PCF) exhibits optical activity, and that the magnitude of the associated circular birefringence increases linearly with twist rate and is highly reproducible. In contrast to previous work on twist-induced circular birefringence, PCF has zero linear birefringence and an on-axis core, making the appearance of circular birefringence rather unexpected. A theoretical model based on symmetry properties and perturbation theory is developed and used to show that both spin and orbital angular momentum play a role in this effect. It turns out that the degenerate left- and right-circularly polarized modes of the untwisted PCF are not 100% circularly polarized but carry a small amount of orbital angular momentum caused by the interaction between the core mode and the hollow channels.

DOI: 10.1103/PhysRevLett.110.143903 PACS numbers: 42.81.Gs, 42.81.Cn

Introduction.—Optical activity (rotation of the elliptical polarization axis) occurs in materials where left- and right-circularly (LC and RC) polarized light have different phase indices; i.e., there is circular birefringence. The relationship between ellipse rotation angle ψ and propagation distance z is given by

$$\psi = \frac{\pi(n_{RC} - n_{LC})}{\lambda} z = \frac{\pi B_C}{\lambda} z, \tag{1}$$

where λ is the wavelength, n_{RC} and n_{LC} are the effective refractive indices of RC and LC polarized modes and B_C is the circular birefringence. Optical fibers with high values of B_C are able to maintain circular polarization state against external perturbations such as bending and mechanical stress and are useful in applications such as electric-current monitoring [1] where it is necessary to suppress polarization scrambling. Circular birefringence can be induced in optical fibers by mechanically twisting a linearly birefringent fiber [2], and by spinning (during the draw) a fiber with an off-axis core [3], a photonic crystal fiber with elliptical hollow channels [4], or a fiber incorporating anisotropic materials [5]. Theory confirms that a similar effect can be induced by incorporating chiral materials into the fiber structure [6].

In a recent paper it was shown that continuously twisted endlessly single-mode (ESM) photonic crystal fibers (PCFs) [7] exhibit dips in their transmission spectrum, associated with coupling to orbital angular momentum resonances in the cladding [8]. Here we show theoretically and experimentally that such fibers exhibit circular birefringence within the high-transmission spectral regions between the transmission dips, despite there being no linear birefringence or anisotropy in the structure. This effect is caused by a subtle interplay between the twisted "six-spoke" modal field pattern and the polarization state. A theoretical model based on symmetry properties and perturbation theory is used to analyze the phenomenon. Excellent agreement is obtained between experiment and theory.

Experiment.—An ESM PCF with hole diameter ~ 1 μm and interhole spacing ~ 3 μm was used in the experiments [see the scanning electron micrograph in Fig. 1(a)]. The twisted PCFs were fabricated by rigidly fixing one end while mounting the other at the center of a motorized rotation stage. While the motor was rotating, a focused continuous-wave CO_2 laser beam was scanned along the fiber using a steering mirror fixed to a motorized linear translation stage. The laser power was chosen to heat the fiber to the glass-softening temperature—any residual torsional stress is relieved when the sample is dismounted. The circular birefringence of three ~ 5 cm long samples with twist rates of 3.1, 6.3, and 10.1 rad/mm were measured using a cut-back method. A tunable continuous-wave Ti:sapphire laser was used as the light source and the polarization states before and after the fiber were measured with a commercial polarimeter.

The results from a series of cut-back measurements with linearly polarized light at a fixed wavelength of 800 nm are plotted in Fig. 1(a). The output polarization state remains predominantly linearly polarized but rotated by an angle ψ, as expected if circular birefringence is present. It is clear from Fig. 1(a) that the rotation angle is linearly proportional to the fiber length and therefore that the value of B_C can be obtained by fitting Eq. (1) to straight lines.

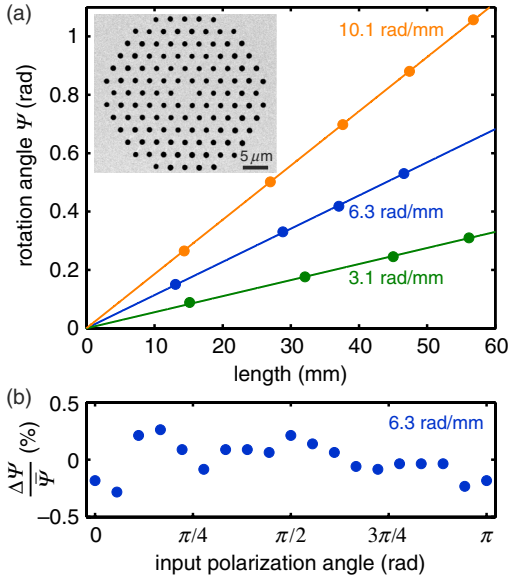

FIG. 1 (color online). (a) Cut-back measurements (circles) and linear regression (lines) of the rotation angle of linear polarization at a fixed wavelength of 800 nm for PCFs with twist rates of 3.1, 6.3, and 10.1 rad/mm, with corresponding beat lengths of 57.1, 27.6, and 16.9 cm. (Inset) Scanning electron micrograph of the PCF. (b) Relative rotation angle deviation of the output polarization state as a function of input polarization angle.

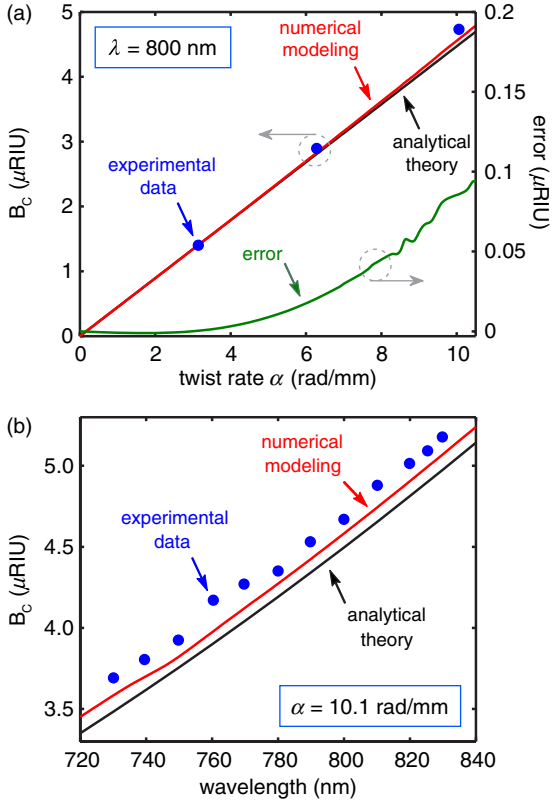

FIG. 2 (color online). (a) Circular birefringence as a function of twist rate at a wavelength of $\lambda_0 = 800$ nm. The error is the difference between the numerically modeled (by solving the full Maxwell equations with a finite element method) and the values of B_C calculated using perturbation theory; (b) B_C as a function of wavelength for a twist rate of 10.1 rad/mm.

The dependence of the output polarization angle on the launched polarization angle was also measured for a sample with a twist rate of 6.3 rad/mm [Fig. 1(b)] and shows a deviation of less than $\pm 0.5\%$. The ellipticity, defined here as the ratio of semiminor to semimajor axis of the polarization states, was measured to be less than 0.05, showing that the circular birefringence is very weakly dichroic. We attribute this to inevitable small deviations from sixfold symmetry in the structure.

The values of B_C at different twist rates are plotted in Fig. 2(a) for the three fibers in Fig. 1(a). A comparison of the experimental results with numerical solutions modeled by a finite element method applied to the full Maxwell equations in a twisted coordinate frame [8] shows excellent agreement; as expected, B_C increases with twist rate. Figure 2(b) shows the measured wavelength dependence of B_C for a twist rate of 10.1 rad/mm. The modal field extends further into the cladding as the wavelength increases, resulting in a larger overlap with the cladding microstructure and increasing the effect.

Theoretical model.—To understand the observed circular birefringence, it is useful to solve Maxwell's equations both in a helicoidal coordinate system [9] and in the Cartesian laboratory frame. The full details of this analysis will be published elsewhere, but, in essence, because the twist rate α (rad/mm) is relatively small (i.e., $\alpha \cdot \Lambda \ll 1$, where Λ is the interhole spacing), Maxwell's equations can be solved using a perturbation approach, based on accurate full-vector numerical solutions for the modal fields in the untwisted fiber.

Modes of untwisted fiber.—The modes of the untwisted fiber fall into two categories: a core mode, which is exponentially localized in the vicinity of the glass core, and cladding modes (commonly referred to as space-filling modes), which are delocalized in the microstructured cladding. Here we are interested only in the core mode. All these modes are eigensolutions of the system $H^{un}\vec{u} = -i\partial_z\vec{u}$, where H^{un} is defined in the paraxial approximation as

$$H^{un} = \frac{\lambda_0}{4\pi n(\rho, \phi, \lambda_0)}\nabla_\perp^2, \tag{2}$$

$\nabla_\perp^2$ is the transverse Laplacian, λ_0 the vacuum wavelength, and $n(\rho, \phi)$ maps the transverse refractive index profile of the fiber. The vector $\vec{u} = (u_x, u_y)$ denotes the electric field vector profile in the transverse direction, which in the case of fiber modes is given by $\vec{u} = \vec{w}(\rho, \phi)\exp(i\Delta\beta_z^{un}z)$, where ρ and ϕ are the radial and azimuthal coordinates and $\beta_z^{un} = \beta_0 + \Delta\beta_z^{un}$ is the modal propagation constant in the untwisted fiber and β_0 is a reference wave vector. The orbital and spin angular momentum operators are

$L = -i\partial_\phi$ and $S = \sigma_2$, where $\sigma_2 = [(0, -i), (i, 0)]$ is the second Pauli matrix; the total angular momentum operator J equals $L + S$.

In an untwisted PCF the hollow channels break the circular symmetry and as a result the expectation value of the total angular momentum, which we denote by $\langle J\rangle$, deviates slightly from ± 1 due to the presence of minor contributions from eigenstates with eigenvalues $j = \pm 1 + 6m$ (this follows from the sixfold rotational symmetry), where m is a positive or negative integer. $\langle J\rangle$ can be separated into spin and orbital angular momentum contributions, which one can calculate from the field distributions (modeled numerically) in the untwisted fiber via the nonparaxial integral expression in Eq. (38) in Ref. [10] [this is more accurate than Eq. (3)]. Numerical calculations based on the finite element method, using both Cartesian and cylindrical coordinates, yielded the same values (to the fourth decimal place) for the individual contributions of spin and orbital angular momenta: $(\langle S\rangle, \langle L\rangle) = \pm(0.9996,\ 0.0022)$ where $(+)$ refers to LC and $(-)$ to RC polarization, i.e., $\langle J\rangle = \pm 1.0018$. The deviation of $\langle S\rangle$ from unity indicates that the modal solutions are not perfectly LC or RC polarized, as might perhaps be expected. Note that in the untwisted fiber the LC and RC modes are degenerate; i.e., their axial propagation constants are identical, which means that no optical activity will be observed, also as expected. Figure 3 shows the axial component of the spin and orbital angular momentum (OAM) densities. The OAM density is nonzero only close to the air holes in the first ring, where significant contributions from the other eigenstates of J are present.

Twisted fibers.—In a twisted fiber, however, the situation gets more complicated and interesting. Upon introducing the ansatz $\vec{u} = \exp(i\alpha z[L + S])\vec{w}(\rho, \phi)\exp(i\Delta\beta_z^{tw} z)$, one can show by perturbation theory that the propagation constant of the core mode, evaluated in a helicoidal reference frame rotating with the twist, can be written

$$\beta_z^{tw} = \beta_z^{un} - \alpha\frac{\int \rho d\rho d\phi\ \vec{w}^\dagger(L + S)\vec{w}}{\int \rho d\rho d\phi\ \vec{w}^\dagger\vec{w}} = \beta_z^{un} - \alpha\langle J\rangle. \quad (3)$$

This indicates that, *in the helicoidal reference frame*, β_z^{tw} is shifted in proportion to its total angular momentum, weighted by $\vec{w}$, in agreement with perturbation theory. This shift is opposite in sign for LC and RC polarized core modes, as confirmed by finite element modeling in Fig. 3 of the paper by Wong *et al.* [8]. The shift in propagation constant in Eq. (3) is reminiscent of Zeeman splitting, in which a magnetic field (analogous in our case with twist rate) induces an electronic energy level shift (analogous with propagation constant) that depends on the total angular momentum. We intend to explore this analogy in more detail in a future publication.

Twisted circular-symmetric fiber.—In a twisted circular-symmetric fiber the modes turn out to be eigenstates of J with integral eigenvalues $j = l + s$ (although l and s themselves are not in general exact integers, their sum is integral [11]). In order to return from the helicoidal to the laboratory frame, a coordinate transformation is necessary. For a circular-symmetric fiber this yields

$$\beta_z^{\text{lab}} = \beta_z^{tw} + \alpha(l + s) = \beta_z^{un}; \quad (4)$$

i.e., the quotient of integrals in Eq. (3) evaluates exactly to the integer $j = (l + s)$ so that the laboratory propagation constant exactly equals that of the untwisted fiber: as expected, twisting has no effect in this case.

Twisted PCF.—In an untwisted PCF we have seen that the fiber mode consists of a linear superposition of all the J eigenstates, with an expectation value $\langle J\rangle$ that is no longer an integer. When the PCF is twisted, Eqs. (3) and (4) lead to the result

$$\beta_z^{\text{lab}} = \beta_z^{un} + \alpha(j - \langle J\rangle) \quad (5)$$

in the laboratory frame, where j is the integral eigenvalue of the J operator corresponding most closely to the total

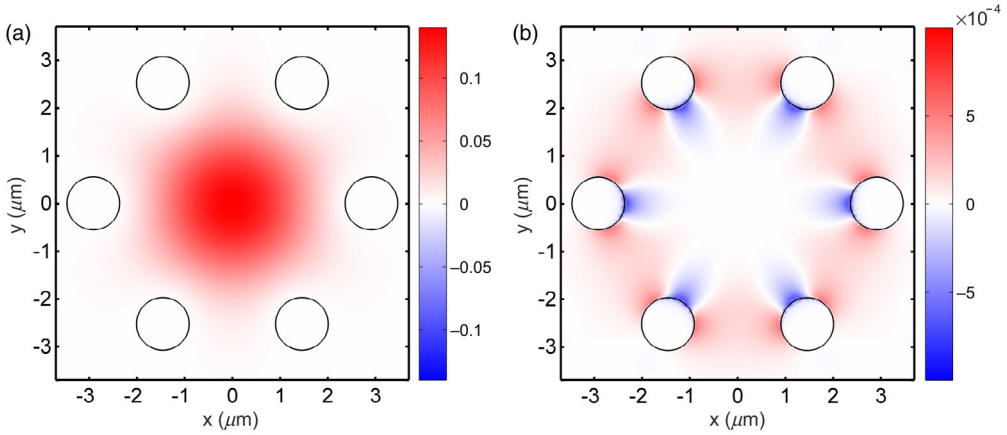

FIG. 3 (color online). (a) Axial component of spin angular momentum density, normalized so that the total energy flux is unity. (b) Normalized axial component of OAM density. Note the small OAM contribution in the vicinity of the fiber core, which leads to a non-negligible contribution to the total angular momentum density and becomes dominant when circular birefringence is considered.

angular momentum of the PCF core mode. Because in our case one of the J eigenstates in the superposition is dominant (the one with eigenvalue j), β_z^{lab} is consistently slightly different from β_z^{un}. It is this small disparity, caused by the presence of small but significant amounts of higher order OAM states, that gives rise to the observed optical activity.

Evaluating β_z^{lab} in Eq. (5) for the LC ($j = +1$) and RC ($j = -1$) polarized modes, and taking the difference of the two values, we finally obtain an expression for the circular birefringence:

$$B_C = n_{RC} - n_{LC} \approx \alpha\lambda_0(\langle J\rangle - j)/\pi. \quad (6)$$

This estimate of B_C, calculated using perturbation theory, is compared in Fig. 2(a) with the value obtained from a full numerical solution of Maxwell's equations. The error is less than 2%.

Conclusions.—In spectral regions where the transmission is high (i.e., away from the transmission dips caused by excitation of orbital resonances in the cladding [8]), continuously twisted ESM PCFs exhibit circular birefringence via a nonresonant geometrical effect that can only be understood if both spin and orbital angular momentum are considered. A theoretical model based on symmetry properties and perturbation theory is in excellent agreement with experimental and numerical data and shows that the circular birefringence is caused by excitation of higher order angular momentum eigenstates by the sixfold symmetric structure around the core. Because the structures are created by thermal postprocessing and not mechanical stress, the value of B_C is not limited by the ultimate strength of the glass [12], and furthermore can be fine-tuned by applying mechanical twist [13]. Such optically active twisted fibers may find applications in polarization control, nonlinear optics, and sensing.

S. M. B. and M. J. P. thank the UK EPSRC, the Royal Society, and the Wolfson Foundation for financial support.

[1] V. P. Gubin, V. A. Isaev, S. K. Morshnev, A. I. Sazonov, N. I. Starostin, Y. K. Chamorovskii, and A. I. Usov, Quantum Electron. **36**, 287 (2006).
[2] R. Ulrich and A. Simon, Appl. Opt. **18**, 2241 (1979).
[3] R. D. Birch, Electron. Lett. **23**, 50 (1987).
[4] A. Argyros, J. Pla, F. Ladouceur, and L. Poladian, Opt. Express **17**, 15 983 (2009).
[5] I. M. Bassett, Opt. Lett. **13**, 844 (1988).
[6] L. Poladian, M. Straton, A. Docherty, and A. Argyros, Opt. Express **19**, 968 (2011).
[7] T. A. Birks, J. C. Knight, and P. St. J. Russell, Opt. Lett. **22**, 961 (1997).
[8] G. K. L. Wong, M. S. Kang, H. W. Lee, F. Biancalana, C. Conti, T. Weiss, and P. St. J. Russell, Science **337**, 446 (2012).
[9] A. Nicolet, F. Zolla, Y. O. Agha, and S. Guenneau, COMPEL - The International Journal for Computation and Mathematics in Electrical and Electronic Engineering; Multilingua **27**, 806 (2008).
[10] S. M. Barnett, J. Opt. B **4**, S7 (2002).
[11] K. Okamoto, *Fundamentals of Optical Waveguides* (Academic Press, Burlington, MA, 2006), 2nd ed.
[12] A. J. Barlow and D. N. Payne, Electron. Lett. **17**, 388 (1981).
[13] G. K. L. Wong, X. M. Xi, M. S. Kang, H. W. Lee, and P. St. J. Russell, in *Frontiers in Optics Technical Digest* (OSA, Washington, DC, 2012), paper FTh3C.